



## Corrosion inhibition effect of hydroxy pyrazoline derivatives on mild steel in sulphuric acid solution together with Quantum chemical studies

N. Anusuya<sup>1</sup>, P. Sounthari<sup>2</sup>, J. Saranya<sup>2</sup>, K. Parameswari<sup>2</sup>, S. Chitra<sup>2\*</sup>

<sup>1</sup>Department of Chemistry, RVS Faculty of Engineering, Coimbatore, India

<sup>2</sup>Department of Chemistry, PSGR Krishnammal College for Women, Coimbatore, India

Received 18 Nov 2014, Revised 13 Mar 2015, Accepted 13 Mar 2015

\*Corresponding author: E-mail: [rajshree1995@rediffmail.com](mailto:rajshree1995@rediffmail.com)

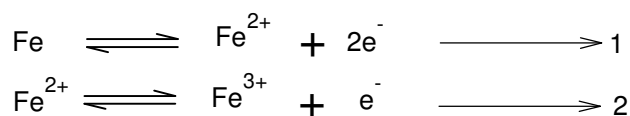
### Abstract

Inhibition potential of synthesized pyrazoline derivatives on the corrosion inhibition of mild steel in 1M H<sub>2</sub>SO<sub>4</sub> solution have been evaluated and studied by gravimetric, Tafel polarization, electrochemical impedance spectroscopy techniques and the quantum chemical studies using density functional theory (DFT). The results showed that the inhibition efficiency of the investigated compounds depend on the concentration and nature of the inhibitor. The effect of temperature on the corrosion behavior of mild steel in 1M H<sub>2</sub>SO<sub>4</sub> without and with the inhibitors was studied in the temperature range 303 to 333 K. Some activated thermodynamic parameters were computed and discussed. Polarization studies showed that all the pyrazolines function as mixed inhibitor, but predominantly act as cathodic type. The surface morphology of inhibited mild steel was analyzed by scanning electron microscope technology with energy dispersive X-ray spectroscopy (SEM-EDX). FT-IR spectroscopic analysis was used to obtain information on bonding mechanism between the metallic surface and the inhibitors. Quantum chemical parameters such as highest occupied molecular orbital energy (E<sub>HOMO</sub>), lowest unoccupied molecular orbital energy (E<sub>LUMO</sub>), energy gap (ΔE) and dipole moment (μ), the softness (σ), the fraction of the electrons transferred from the inhibitor to the metal surface (ΔN) and the total energy (TE) have been calculated. It was found that theoretical data support the experimental results.

**Keywords:** Pyrazoline derivatives, mild steel, acid corrosion, thermodynamic parameters, density functional theory.

### 1. Introduction

Iron and steel alloys have been widely used in huge applications due to their properties. Corrosion of iron due to the contact with harsh environments presents a serious economic problem. It has been reported [1-3] that the corrosion of iron in corrosive solutions occurs through the dissolution of iron initially from Fe (0) into Fe (II) and further to Fe (III).



The corrosion and corrosion inhibition of iron in different environments have been reported in many research studies [4]. One of the most important methods to protect metals and alloys including iron against corrosion in a corrosive medium is the use of corrosion inhibitors [5]. Azole derivatives have been reported to be effective inhibitors against corrosion of metals in corrosive media [6]. The effectiveness of these compounds depends on its functional groups steric effects, electronic density of donor atoms and P-orbital character of donating electrons [7, 8]. The inhibition mechanism usually invokes their interactions with the metallic surfaces via their adsorption sites where polar functional groups are usually regarded as the reaction centres and where the inhibitor molecules get bonded to the metal surface by chemisorption, physisorption or complexation with the polar groups acting as the reaction centres in the molecules [9].

The present work is aimed to investigate the role played by newly synthesized hydroxy pyrazoline derivatives on the corrosion inhibition of mild steel in 1M H<sub>2</sub>SO<sub>4</sub>. The molecular design of the new compounds was based on the fact that, the synthesized hydroxy pyrazolines containing –NH, –OH, >C=O, >C=S, phenyl groups would contribute more effectively towards inhibition of corrosion of mild steel in acid media.

The inhibitory action has been investigated using weight loss measurements, the adsorption mechanism of the inhibitor on the mild steel surface in 1M H<sub>2</sub>SO<sub>4</sub> solution was discussed. The effect of temperature on

corrosion and inhibition processes was also assessed. Theoretical calculations were further employed to explain the inhibition efficiency of synthesized hydroxy pyrazoline derivatives as corrosion inhibitors.

## 2. Experimental methods

### Mild steel specimens and electrode

Cold rolled mild steel specimen of size 1cm x 3cm x 0.08cm having composition 0.084% C, 0.369% Mn, 0.129% Si, 0.025% P, 0.027% S, 0.022% Cr, 0.011% Mo, 0.013% Ni and the remainder iron were used for weight loss measurements. For electrochemical methods, a mild steel rod of same composition with an exposed area of 0.785 cm<sup>2</sup> was used. The specimens were polished with 1/0, 2/0, 3/0 and 4/0 grades of emery sheets and degreased with trichloroethylene and dried using a drier. The plates were kept in a desiccator to avoid the absorption of moisture.

### 2.1 Synthesis of inhibitors

#### (i) Synthesis of chalcones (I)

Chalcones were prepared by reacting a mixture of acetanilide (0.05 mol), benzaldehyde (0.05 mol), aqueous sodium hydroxide (10%, 5 ml) and methanol (50 ml). The reaction mixture was stirred for 10 hour at room temperature using magnetic stirrer. It was further refluxed for 6 hour on a water bath. After completion of the reaction, the excess solvent was removed by distillation and the resultant viscous mass was poured into ice water (100 ml) with vigorous stirring and left overnight for complete precipitation. The resultant yellow coloured solid was filtered, washed with cold water, dried and recrystallized from ethanol [10].

#### (ii) Synthesis of dibromchalcone (II)

To the Chalcone I (0.1 mol) in acetic acid (10 ml), bromine (0.125 mol) in acetic acid (10 ml) was added slowly with stirring at 0°C. After complete addition of bromine solution, the reaction mixture was stirred for 5 hour. The solid obtained was filtered and recrystallized from acetone [11].

#### (iii) Synthesis of acid hydrazides (III<sub>a-c</sub>)

Hydrazine hydrate and methyl benzoate were taken in 1:1 ratio and few ml of alcohol was added to it. This solution was heated in a water bath for half an hour. It was cooled. The precipitated acid hydrazide obtained was filtered, washed and dried. Similar procedure was followed for methyl anthranilate and methyl salicylate.

#### (iv) Synthesis of hydroxy pyrazolines (IV<sub>a-d</sub>)

A mixture of dibromo chalcone II (4.04 g, 0.01 mol), substituted benzohydrazide (0.012 mol) and triethylamine (3 ml) was heated under reflux in absolute ethanol (15 ml) for 8 hour. The reaction mixture was cooled and poured into ice-cold water. The solid separated was filtered, dried and recrystallized from ethanol [11].

[5-hydroxy-3-phenyl-5-(phenylamino)-4,5-dihydro-1H-pyrazol-1-yl](phenyl)methanone (PPM) IV<sub>a</sub>: Yield: 92%, Colour: brown, IR spectrum ( $\gamma/\text{cm}^{-1}$ ): 3198.11 (OH); 1620.27 (C=O), 1538.30, 1531.55 (C=N).

(2-hydroxyphenyl)[5-hydroxy-3-phenyl-5-(phenylamino)-4,5-dihydro-1H-pyrazol-1-yl]methanone (PHPM) IV<sub>b</sub>: Yield: 88%, Colour: brown, IR spectrum ( $\gamma/\text{cm}^{-1}$ ): 3260.80 (OH); 1739.87 (C=O), 1538.30, 1634.74 (C=N).

(2-aminophenyl)[5-hydroxy-3-phenyl-5-(phenylamino)-4,5-dihydro-1H-pyrazol-1-yl]methanone (PAPM) IV<sub>c</sub>: Yield: 80%, Colour: brown, IR spectrum ( $\gamma/\text{cm}^{-1}$ ): 3192.33 (OH); 3316.74 (NH<sub>2</sub>); 1737.94(C=O), 1600.99 (C=N).

5-hydroxy-3-phenyl-5-(phenylamino)-4,5-dihydro-1H-pyrazole-1-carbothioamide (PCT) IV<sub>d</sub>: Yield: 75%, Colour: brown, IR spectrum ( $\gamma/\text{cm}^{-1}$ ): 3180.75 (OH); 3259.84 (NH<sub>2</sub>); 1220.03(C=S), 1655.96(C=N).

### 2.2 Non-Electrochemical measurements

#### 2.2.1 Weight loss method

The simplest and most accurate method for estimating the corrosion rate is weight loss analysis. The initial weight of the polished specimen was taken. The solutions were taken in 100 ml beakers and the specimens were suspended in triplicate into the solution using glass hooks. Care was taken to ensure the complete immersion of the specimen. After a period of three hours, the mild steel samples were taken out, washed with distilled water,

dried and weighed to the accuracy of four decimals. From the initial and final mass of the specimen, (i.e before and after immersion in the solution) the loss in weight was calculated. The experiment was repeated for various concentrations of the hydroxy pyrazolines (IV<sub>a-d</sub>). The inhibition efficiency, corrosion rate and surface coverage were calculated from the weight loss results using the formulas,

$$\text{Inhibitor Efficiency, (IE \%)} = \frac{(\text{Weight loss without inhibitor} - \text{Weight loss with inhibitor})}{\text{Weight loss without inhibitor}} \times 100$$

$$\text{CorrosionRate, CR} = \frac{534 \times \text{Weightloss (g)}}{\text{Density} \times \text{Area (cm)} \times \text{Time (hr)}}$$

$$\text{SurfaceCoverage } \theta = \frac{(\text{Weight loss without inhibitor} - \text{Weight loss with inhibitor})}{\text{Weight loss without inhibitor}}$$

In order to investigate the effect of temperature on the inhibitor performance, the above procedure was carried out in the different temperature range i.e., 303 K – 333 K with one hour immersion time, using a thermostat, with the inhibitor concentration of 10 mM. Activation energy ( $E_a$ ), free energy of adsorption ( $\Delta G^0$ ), enthalpy and entropy ( $\Delta H^0$  &  $\Delta S^0$ ) were calculated using the formula,

$$\log CR = \frac{-E_a}{2.303RT} + \log A \quad \longrightarrow \quad (1)$$

$$K = \frac{\theta}{C(1-\theta)} \quad \longrightarrow \quad (2)$$

where,  $\theta$  = Surface coverage of the inhibitor,  $C$  = Concentration of the inhibitor in mM/100  $\mu$ l.

Therefore,

$$CR = \frac{RT}{Nh} \exp \frac{\Delta S^0}{R} \exp \frac{-\Delta H^0}{RT} \quad \longrightarrow \quad (3)$$

Where  $R$  is the gas constant,  $T$  is the temperature,  $N$  is the Avogadro's number and  $h$  is the Planck's constant. A plot of  $\log (CR/T)$  versus  $1/T$  should produce a straight line with slope equal to  $(-\Delta H^0/(2.303R))$  and intercept equal to  $[\log(R/Nh) + (\Delta S^0/(2.303R))]$ .

### 2.2.2 Atomic Absorption Spectrophotometric studies

The weight loss can also be determined by the amount of metal dissolved in the solution using atomic absorption spectroscopy (AAS). Atomic absorption spectrophotometer (model GBC 908, Australia) was used for estimating the amount of dissolved iron in the corrodent solution containing various concentrations of inhibitors in 1M  $H_2SO_4$  after exposing the mild steel specimens for 3 hour. From the amount of dissolved iron, the inhibition efficiency was calculated.

$$\text{Inhibition Efficiency (\%)} = \left( \frac{B - A}{B} \right) \times 100$$

where  $A$  and  $B$  are the amount of dissolved iron in presence and absence of inhibitor.

### 2.3 Electrochemical Techniques

The electrochemical impedance measurements were carried out for mild steel in acidic media using computer controlled potentiostat. (IVIUM Compactstat Potentiostat/Galvanostat). After immersion of the specimen prior to the impedance measurement, a stabilization period of 30 minutes was observed for  $E_{oc}$  to attain a stable value. The impedance measurements were made at corrosion potentials over a frequency range of 10 KHz to 0.01Hz with a signal amplitude of 10mV. The real part ( $Z'$ ) and the imaginary part ( $Z''$ ) were measured at various frequencies. A plot of  $Z'$  Vs  $Z''$  were made. From the plot, the charge transfer resistance ( $R_t$ ) and double layer capacitance ( $C_{dl}$ ) were calculated.

$$\text{Inhibition Efficiency (\%)} = \frac{R_{ct}^* - R_{ct}}{R_{ct}^*} \times 100$$

Where,  $R_{ct}$  = charge transfer resistance in the presence of inhibitor;  $R_{ct}^*$  = charge transfer resistance in the absence of inhibitor.

Polarization measurements were made after EIS studies in the same cell set up for a potential range of -200 mV to +200 mV with respect to open circuit potential at a sweep rate of 1mV/sec. From the plot, the

inhibition efficiency, Tafel slopes corrosion potentials and corrosion current were calculated using IVIUM software.

$$\text{Inhibition Efficiency (\%)} = \frac{I_{\text{corr}} - I_{\text{corr(inh)}}}{I_{\text{corr}}} \times 100$$

where  $I_{\text{corr}}$  and  $I_{\text{corr(blank)}}$  are the corrosion current density values without and with inhibitors respectively.

### 2.4 Surface morphology

#### 2.4.1 Scanning electron microscope-energy dispersive X-ray spectroscopy (SEM-EDX)

Scanning electron microscopy (SEM) was used to study the surface morphology of the mild steel specimen. The surface morphology of the samples, after 3 hour immersion in 1M H<sub>2</sub>SO<sub>4</sub> solutions in presence of selected concentration of various inhibitors studied, was performed on Medzer biomedical research microscope.

#### 2.4.2 Surface examination study

Mild steel specimens were immersed in selected concentrations of the inhibitors for a duration of 3 hours. After 3 hours, the specimens were taken out and dried. The surface of the metal specimen was analyzed by Fourier transform infrared spectra using FTIR-Affinity1 (Shimadzu).

## 3. Results and Discussion

### 3.1 Non-Electrochemical methods

#### 3.1.1 Weight loss measurements

Weight loss of mild steel surface in 1M H<sub>2</sub>SO<sub>4</sub> was determined at 303, 313, 323 & 333 K in the absence and presence of different concentrations of hydroxy pyrazolines (PPM-PPCT). The obtained corrosion parameters are presented in Table 1 & 2.

**Table 1:** Inhibition efficiencies at various concentrations of inhibitors for the corrosion of mild steel in 1M H<sub>2</sub>SO<sub>4</sub> obtained by weight loss measurements at 30±1°C.

Name of the Inhibitor	Inhibitor Concentration (mM)	Weight Loss (g)	Inhibition Efficiency (%)	Corrosion Rate (mpy)	Surface Coverage (θ)
Blank		0.2059	-	13.34	-
PPM	0.5	0.1554	24.53	10.07	0.2453
	1	0.1164	43.47	7.54	0.4347
	2.5	0.0889	56.82	5.76	0.5682
	5	0.0678	67.07	4.39	0.6707
	7.5	0.0396	80.07	2.57	0.8077
	10	0.0276	86.60	1.79	0.8660
PHPM	0.5	0.0925	55.08	5.99	0.5508
	1	0.0818	60.27	5.30	0.6027
	2.5	0.0576	72.03	3.73	0.7203
	5	0.0390	81.06	2.53	0.8106
	7.5	0.0295	85.67	1.91	0.8567
	10	0.0179	91.31	1.16	0.9131
PAPM	0.5	0.0753	63.43	4.88	0.6343
	1	0.0452	78.05	2.93	0.7805
	2.5	0.0217	89.46	1.41	0.8946
	5	0.0169	91.79	1.09	0.9179
	7.5	0.0111	94.61	0.72	0.9461
	10	0.0049	97.62	0.32	0.9762
PCT	0.5	0.0783	61.97	5.07	0.6197
	1	0.0536	73.97	3.47	0.7397
	2.5	0.0171	91.69	1.11	0.9169
	5	0.0122	94.07	0.79	0.9407
	7.5	0.0068	96.70	0.44	0.9670
	10	0.0035	98.30	0.23	0.9830

It is clear from the table that the percentage inhibition efficiency increases with concentration of the inhibitors and decreases with temperature. The compounds exhibited a maximum inhibition efficiency of 80-98% at a concentration of 10mM. The increase in inhibition efficiency with increasing concentrations of the inhibitors at room temperature (303K) is due to an increase in surface coverage resulting in retardation of the metal dissolution [12]. The efficiency of the inhibitors follow the order

$$\text{PCT} > \text{PAPM} > \text{PHPM} > \text{PPM}$$

The data in Table 1 reveal that a maximum efficiency of 98.30% was obtained in the presence of 10 mM for PCT respectively. All the inhibitors have a pyrazole ring, 3 phenyl ring, -NH, >C=O and -OH groups. In addition to these groups, the inhibitor PCT has -NH<sub>2</sub>, -C=S and but one aryl group less. The maximum inhibition efficiency of the compound PCT is due to the presence of >C=S group [13]. According to Every and Riggs [14], organic compounds containing nitrogen and sulphur have better inhibition efficiency in acidic media compared to the organic compound containing nitrogen or sulphur. PAPM exhibit an inhibition efficiency of 97.62%, which is attributed to the electron releasing nature of NH<sub>2</sub>group.

### 3.1.2 Effect of temperature

Temperature has more pronounced effect on the rate of electrochemical corrosion of the metal. The effect of temperature on the inhibited acid-metal reaction is very complex. Many changes such as rapid etching, desorption of inhibitor as well as inhibitor decomposition occur on the metal surface [15]. The results in Table 2 reveal that an increase in temperature decreases the inhibition efficiency. Generally, the metallic corrosion in acidic media is accompanied with evolution of hydrogen gas and rise in temperature usually accelerates the corrosion reactions resulting in higher dissolution rate of the metal [16]. A decrease in inhibition efficiency with temperature can be attributed to the increased desorption of inhibitor molecules from the metal surface or decreased adsorption process suggesting physical adsorption mode. But there are cases where chemical adsorption occurs, although inhibition efficiency decreases with increasing temperature [17].

**Table 2:** Inhibition efficiencies at 10mM Concentration of inhibitors for the corrosion of mild steel in 1M H<sub>2</sub>SO<sub>4</sub> obtained by Weight loss measurements at higher temperature.

Name of the Inhibitor	Temperature (K)	Weight Loss (g)	Inhibition Efficiency (%)	Corrosion Rate (mpy)	Surface Coverage (θ)
PPM	303	0.0120	82.51	2.33	0.8251
	313	0.0316	81.39	6.14	0.8139
	323	0.0938	66.74	18.23	0.6674
	333	0.1882	52.08	36.58	0.5208
PHPM	303	0.0105	84.69	2.04	0.8469
	313	0.0461	72.85	8.96	0.7285
	323	0.0923	67.27	17.94	0.6727
	333	0.1993	49.25	38.74	0.4925
PAPM	303	0.0016	97.67	0.31	0.9767
	313	0.0052	96.94	1.01	0.9694
	323	0.0121	95.71	2.35	0.9571
	333	0.0346	91.19	6.72	0.9119
PCT	303	0.0006	99.13	0.12	0.9913
	313	0.0024	98.59	0.47	0.9859
	323	0.0060	97.87	1.17	0.9787
	333	0.0139	96.46	2.70	0.9646

The activation energy E<sub>a</sub> for mild steel in 1M H<sub>2</sub>SO<sub>4</sub> in the absence and presence of inhibitors were calculated from the Arrhenius equation (Eq.1) and presented in Table 3.

Fig 1 represents the Arrhenius plot of log C<sub>R</sub> vs 1000/T for uninhibited and inhibited solutions. The E<sub>a</sub> values were calculated from the slopes of the Arrhenius plots. From Table 3 it is evident that the E<sub>a</sub> values are higher in the presence of inhibitors (78-87 K<sup>J mol<sup>-1</sup></sup>) compared to blank (48.45 K<sup>J mol<sup>-1</sup></sup>). This is attributed to physical adsorption, where chemical adsorption is more pronounced in the opposite case.

The relationship between temperature, percentage inhibition efficiency and  $E_a$  in the presence of inhibitors is as follows [18]

- (i) For inhibitor, whose percentage inhibition efficiency decreases with increase in T,  $E_a$  will be greater than blank.
- (ii) For inhibitors, whose percentage inhibition efficiency does not change with temperature,  $E_a$  will not change in presence or absence of inhibitors.
- (iii) For inhibitors, whose percentage inhibition efficiency increases with increase in temperature, the value of  $E_a$  will be less in inhibited solutions compared to uninhibited solutions.

**Table 3:** Kinetics/Thermodynamic Parameters of mild steel corrosion in 1M  $H_2SO_4$ .

Name of the Inhibitor	$E_a$ kJ	$\Delta H^0$ (kJ mol <sup>-1</sup> )	$\Delta S^0$ (kJ mol <sup>-1</sup> )	$\Delta G^0$ (kJ mol <sup>-1</sup> )			
				303 K	313 K	323 K	333 K
Blank	48.45	-45.81	-0.95	-	-	-	-
PPM	78.51	-75.87	-0.86	-8.23	-8.30	-6.47	-4.98
PHPM	80.24	-77.60	-0.86	-8.63	-7.03	-6.54	-4.66
PAPM	84.48	-81.84	-0.86	-13.73	-13.45	-12.95	-11.22
PCT	87.03	-84.39	-0.86	-16.24	-15.51	-14.89	-13.90

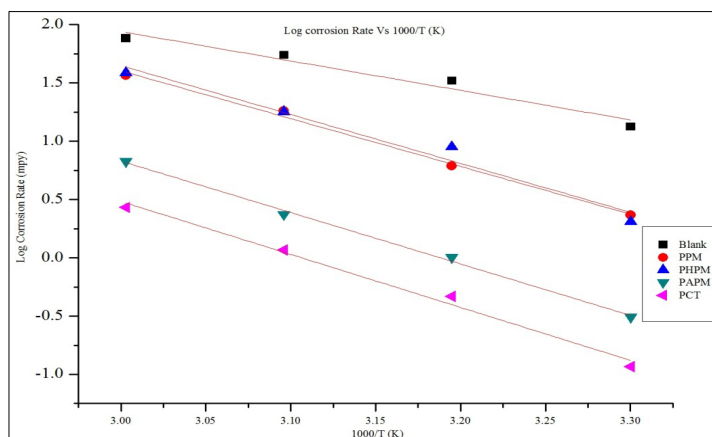
As adsorption decreases more desorption of inhibitor molecules occur because these two opposite processes are in equilibrium. Due to more desorption of inhibitor molecules at higher temperatures, greater surface area of mild steel comes in contact with aggressive environment resulting in an increase in corrosion rates with temperature. The increase in  $E_a$  values confirms stronger physisorption of the inhibitors on the mild steel surface. Physisorption is small but important because it is the preceding stage of chemisorption [19].

#### Thermodynamic parameters

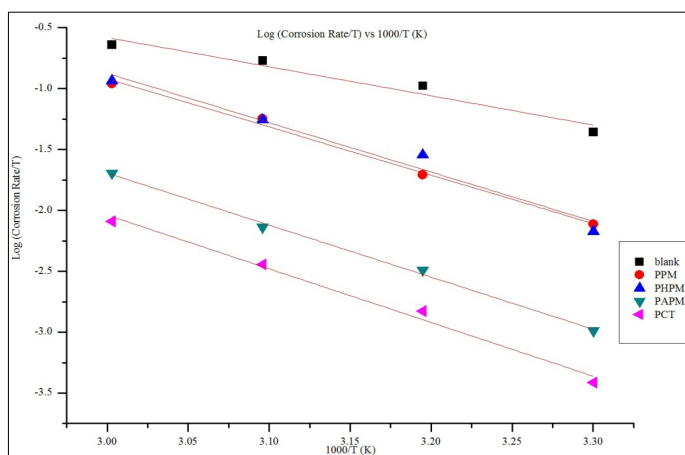
The thermodynamic functions such as the free energy of adsorption ( $\Delta G^0$ ), the enthalpy of adsorption ( $\Delta H^0$ ) and the entropy of adsorption ( $\Delta S^0$ ) are very important to explain the adsorption phenomenon of inhibitor molecule. In order to calculate activation parameters for the corrosion process, Transition State equation (Eq.3) was used.

Fig. 4 shows a plot of  $\log CR/T$  as a function of  $1000/T$  for mild steel in 1M  $H_2SO_4$  in the absence and presence of pyrazolines. Straight lines were obtained with a slope  $\Delta H^0 / 2.303R$  and intercept  $[\log(R/Nh) + (\Delta S^0/2.303R)]$  from which the values of  $\Delta H^0$  and  $\Delta S^0$  were computed and listed in Table 3. The values of enthalpy of activation  $\Delta H^0$  for mild steel in 10 mM of the corrosion inhibitor is higher (75.87-84.39 KJ/mol) than that without the corrosion inhibitor i.e blank (45.81KJ/mol). This is due to the presence of energy barrier for the reaction, which is the corrosion inhibitor adsorption process that has lead to the higher value of  $\Delta H^0$  [20]. The negative sign of  $\Delta H^0$  reveals that the adsorption of the inhibitor molecules is an exothermic process. Generally an exothermic adsorption process suggests either physisorption or chemisorption, while endothermic process is attributed to chemisorption [21].  $\Delta H^0$  values lower than 40KJ/mol indicate physical adsorption and values approaching 100 KJ/mol indicate chemical adsorption [22]. In the present case  $\Delta H^0$  values range from -75.87 to -84.39  $k^J mol^{-1}$  confirming the possibility for chemisorption. In general the large negative  $\Delta H^0$  values confirm both physisorption and chemisorption process.

The negative values of  $\Delta G_{ads}^0$  ensures the spontaneity of the adsorption processes and stability of the adsorbed layer on the steel surface. Generally, values of  $\Delta G_{ads}^0$  around -20 kJ/mol or lower are consistent with the electrostatic interaction between the charged molecules and the charged metal (physisorption); those around -40 kJ/mol or higher involves sharing or transfer from organic molecules to the metal surface to form a coordinate type of bond (chemisorption). In the present case  $\Delta G_{ads}^0$  values are below -20 kJ/mol confirming physisorption whereas  $\Delta H^0$  values confirm chemisorption. This indicates that adsorption of inhibitors on the mild steel surface is neither physisorption or chemisorption, but it is a complex mixed type.



**Fig 1:** Arrhenius plot of corrosion rate of mild steel in 1M H<sub>2</sub>SO<sub>4</sub> solution in absence and presence of inhibitors.



**Fig 2:** Transition plot of log(corrosion rate/T) Vs 1000/T in 1M H<sub>2</sub>SO<sub>4</sub> solution in absence and presence of inhibitors.

The entropy of activation  $\Delta S^\circ$  was negative both in the absence and presence of the pyrazolines implying that the activated complex represented the rate-determining step with respect to the association rather than the dissociation step. This implies that a decrease in disorder occurred when proceeding from the reactants to the activated complex. In addition, the less negative value of  $\Delta S^\circ$  in the presence of pyrazolines implies that the presence of inhibitor created a near-equilibrium corrosion system state.

(ii) Adsorption isotherm

As known that organic inhibitors establish their inhibition via the adsorption of the inhibitor molecules onto the metal surface. The adsorption process is influenced by the chemical structures of the organic compounds, the distribution of charge in a molecule, the nature and surface charge of metal and the type of aggressive media [23]. Generally, inhibitors may function by physisorption, chemisorptions or by complexation with metal ions. Pyrazoline molecules have adsorbed onto the mild steel surface due to vander waals forces. The presence of extensively delocalized  $\pi$ -electrons of the phenyl rings and presence of lone pair of electrons on N, O atoms have favoured greater adsorption [24]. The adsorption isotherm type can provide additional information about the properties of the tested compounds. In this study, the surface coverage is estimated from weight loss measurements to make the fitting and select the suitable isotherm. The following adsorption isotherms are the most common models to study the mechanism of corrosion inhibition [25]

Temkin adsorption isotherm,

$$\text{Exp}^{-2a\theta} = K_{\text{ads}} C \quad \longrightarrow \quad 4$$

Langmuir adsorption isotherm,

$$\frac{C}{\theta} = \frac{1}{k_{ads}} + C \longrightarrow 5$$

El-Awady adsorption isotherm,

$$\log \left( \frac{\theta}{1-\theta} \right) = \log K + y \log C_{inh} \longrightarrow 6$$

Flory–Huggins adsorption isotherm,

$$\log \frac{\theta}{C} = \log K_{ads} + x \log (1 - \theta) \longrightarrow 7$$

where  $K_{ads}$  is the equilibrium constant of the adsorption process,  $C_{inh}$  is the inhibitor concentration,  $f$  is the factor of energetic inhomogeneity and the parameter ‘a’ in El-awady and Flory–Huggins adsorption isotherm is the number of water molecules replaced by inhibitor molecules on metal surface.

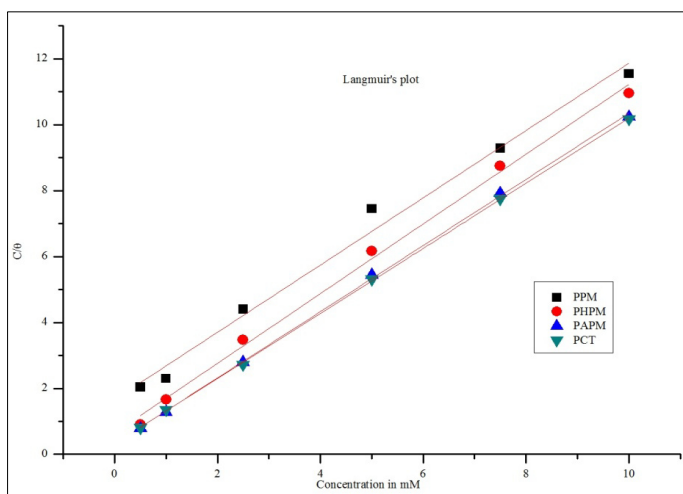


**Fig 3:** Langmuir plot of inhibitors in 1M H<sub>2</sub>SO<sub>4</sub>

For each inhibitor, a Temkin, Langmuir, El-Awady and Flory–Huggins isotherm were fitted. The phenomenon of interaction between the metal surface and the inhibitor can be better understood in terms of the adsorption isotherm. The relationship between  $C / \theta$  and  $C$  (Langmuir isotherm) for the pyrazolines yield a straight line with an approximately unit slope, indicating that the inhibitor under study obeys the Langmuir adsorption isotherm [26]. According to this isotherm,  $\theta$  is related to the inhibitor concentration  $C$  and adsorption equilibrium constant  $K_{ads}$  via:

$$\frac{C}{\theta} = \frac{1}{K_{ads}} + C \longrightarrow 8$$

From the intercepts of the straight lines  $C/\theta$  vs.  $C$ , the equilibrium constant values of the adsorption process,  $K_{ads}$  can be determined. This constant is related to the standard Gibb’s free energy of adsorption ( $\Delta G_{ads}^0$ ) using the following equation

$$\Delta G_{ads}^0 = -RT \ln (55.5 K_{ads}) \longrightarrow 9$$

where 55.5 represent the molar concentration of water in solution ( $\text{mol L}^{-1}$ ),  $R$  is the universal gas constant and  $T$  is the absolute temperature. Table 4 represents the results derived from the application of Langmuir relationship, where the adsorption parameters were recorded for the pyrazolines. From the results obtained, it is significant to note that the  $r^2$  values and the slope values of the plots are very close to unity, which indicates a strong adherence of the adsorption data to the assumptions establishing Langmuir adsorption isotherm. The free energy of adsorption ( $\Delta G_{ads}^0$ ) can be calculated. It is well known that  $\Delta G_{ads}^0$  values on the order of  $-20 \text{ kJ mol}^{-1}$  or less indicate a physisorption, while those more negative than  $-40 \text{ kJ mol}^{-1}$  involve charge sharing or transfer from the inhibitor molecules to the metal surface to form a coordinate chemical bond

(chemisorptions), while values between  $-20 \text{ kJ mol}^{-1}$  and  $-40 \text{ kJ mol}^{-1}$  indicate both physisorption and chemisorption [25]. In this study,  $\Delta G_{ads}^0$  values of pyrazolines were between  $25.69 - 30.64 \text{ kJ mol}^{-1}$ . This value indicated that adsorption of pyrazolines occurs via both chemisorption and physisorption [25].

**Table 4:** Linear correlation coefficients and adsorption parameters for Langmuir relationship for the corrosion of mild steel in  $1\text{M H}_2\text{SO}_4$  at  $30\pm 1^\circ\text{C}$

Name of the inhibitor	Slope	Linear coefficient regression ( $R^2$ )	$K_{ads}$ ( $\text{mol lt}^{-1}$ )	$\Delta G^0$ ( $\text{kJ mol}^{-1}$ )
PPM	1.02	0.9871	0.6010	-26.24
PHPM	1.06	0.9959	1.5474	-28.62
PAPM	1.00	0.9994	3.1967	-30.45
PCT	0.99	0.9998	3.0583	-30.34

### 3.3.2. Atomic absorption spectroscopic studies

The amount of iron dissolved in the presence of isoxazolines when mild steel specimens were exposed to  $1\text{M H}_2\text{SO}_4$  were calculated and presented in Table 5. It has been found that the amount of dissolved iron in the corrodent solution decreases with increase in concentration of the inhibitors and there is good agreement between values of percentage inhibition efficiency calculated from weight loss and AAS technique.

**Table 5:** Amount of dissolved iron present in the corrosive solution with and without inhibitors in  $1\text{M H}_2\text{SO}_4$  measured using atomic absorption spectroscopy.

Name of the inhibitor	Inhibitor concentration (mM)	Amount of iron content ( $\text{mg lt}^{-1}$ )	Inhibition efficiency (%)
Blank	-	1304.96	-
PPM	0.5	998.4	23.49
	10	198.5	84.79
PHPM	0.5	604.1	53.71
	10	128	90.19
PAPM	0.5	498.6	61.79
	10	48.1	96.31
PCT	0.5	532	59.23
	10	28.8	97.79

### 3.3.3. Electrochemical measurements

#### 3.3.3.1 Potentiodynamic polarization measurements

Polarization measurements are suitable for monitoring the progress and mechanisms of the anodic and cathodic partial reaction [27]. Potentiodynamic polarization experiments were undertaken to determine the effect of the anodic ( $\text{Fe} \longrightarrow \text{Fe}^{2+} + 2\text{e}^-$ ) and cathodic ( $2\text{H}^+ + 2\text{e}^- \longrightarrow \text{H}_2$ ) partial reactions of the corrosion process. Typical potentiodynamic polarization curves for the mild steel specimens in  $1\text{M H}_2\text{SO}_4$  without and with different concentrations of hydroxy pyrazolines (PPM – PCT) are shown in Fig 4. The polarization curves reveal that the mild steel specimen exhibit active dissolution with no distinctive transition to passivation within the studied potential range in the acidic environment. The plots also show that the anodic and cathodic reactions in blank acid and upon addition of the pyrazolines follow Tafel’s law. The linear Tafel segments of the anodic and cathodic curves were extrapolated to corrosion potential to obtain the corrosion current densities ( $I_{corr}$ ). The corresponding electrochemical parameters namely corrosion current densities ( $I_{corr}$ ), corrosion potential ( $E_{corr}$ ), the cathodic Tafel slope ( $b_c$ ) and the anodic Tafel slope ( $b_a$ ) derived from the polarization curves are presented in Table 6. Results in the Table 6 indicate that the corrosion current density decreased markedly in the presence of inhibitors compared to the blank solution. The decrease is due to the

blocking of the mild steel surface by adsorption of the inhibitor molecules through active centres. This is evident from the shift of  $E_{corr}$  in the negative direction with respect to blank signifying the suppression of the cathodic reaction. The addition of the inhibitors to the aggressive medium have changed the values of both  $b_a$  and  $b_c$  but  $b_c$  to a greater extent. This indicates that the inhibitors have affected the anodic dissolution of iron as well as cathodic evolution of hydrogen. The mixed nature of the inhibitors can be explained in terms of a change in  $E_{corr}$  values in the presence of inhibitors. If the displacement in  $E_{corr}$  values in the presence of inhibitors is more than  $\pm 85\text{mV/SCE}$  related to  $E_{corr}$  of blank, the inhibitor can be considered as anodic or cathodic [27,28]. If the change in  $E_{corr}$  is less than  $\pm 85\text{mV}$ , the corrosion inhibitor may be regarded as a mixed type. The maximum displacement in our study is  $47\text{mV/SCE}$  which indicates that the pyrazolines act as mixed type inhibitors. However, the minor shift of  $E_{corr}$  values towards negative direction suggests the predominant cathodic control over the reaction.

**Table 6:** Corrosion parameters for mild steel with selected concentrations of the inhibitors in 1M  $\text{H}_2\text{SO}_4$  by Potentiodynamic Polarization Method

Name of the Inhibitor	Concentration (mM)	Tafel Slopes (mV/decade)		$E_{corr}$ (mV)	$I_{corr}$ ( $\mu\text{A cm}^{-2}$ )	Inhibition Efficiency (%)
		$b_a$	$b_c$			
Blank	-	52	112	-467.4	1567.3	-
PPM	0.5	70	137	-491	417.3	73.36
	5	66	164	-485.9	320.0	79.57
	10	62	169	-481.1	279.0	82.19
PHPM	0.5	71	146	-490.9	393.4	74.89
	5	60	163	-479.9	249.3	84.09
	10	53	191	-469.7	216.2	86.20
PAPM	0.5	91	105	-515.6	841.9	46.27
	5	57	118	-506.9	257.3	83.58
	10	25	127	-479.7	164.6	89.49
PCT	0.5	82	137	-509.8	833.2	46.82
	5	58	124	-525	236.3	84.92
	10	45	151	-491	151.6	90.32

### 3.3.3.2 Electrochemical Impedance Spectroscopy (EIS) Measurements

The results of the potentiodynamic polarization experiments were confirmed by impedance measurements, since the electrochemical impedance spectroscopy (EIS), is a powerful technique in studying corrosion mechanisms and adsorption phenomena. EIS measurements were carried out for corrosion of mild steel in 1M  $\text{H}_2\text{SO}_4$  in the absence and presence of pyrazolines (PPM-PCT) at  $30 \pm 1^\circ\text{C}$ . The Nyquists plot for mild steel in the absence and presence of pyrazolines (PCT) are presented in (Fig. 5). It has been reported by Jones etal [29] that the semicircles at high frequencies are generally associated with the relaxation of electrical double-layer capacitors, and the diameters of the high-frequency capacitive loops can be considered as the charge-transfer resistance. The diagram of the capacitive loop obtained increases in the presence of inhibitor and was indicative of the degree of inhibition of the corrosion process. The high frequency limits corresponding to the solution resistance  $R_s$  ( $\Omega$ ), while the lower frequency limits corresponds to  $(R_{ct} + R_s)$ . The low frequency contribution showed the kinetic response of the charge transfer reaction (Mansfeld, 1990) [30]. The impedance parameter such as charge transfer resistance ( $R_{ct}$ ), double layer capacitance ( $C_{dl}$ ) and inhibition efficiency (% IE) were calculated and are listed in Table 7. The charge transfer resistance ( $R_{ct}$ ) values were calculated from the difference in real impedance ( $Z_r$ ) at lower and higher frequencies [31]. The double layer capacitance can be determined from the relationship [31]

$$C_{dl} = \frac{1}{2\pi R_{ct} f(-Z_i \max)}$$

where  $f(-Z_i \max)$  is the frequency at which the imaginary part of the impedance is a maximum.  $R_{ct}$  and  $C_{dl}$  derived from the impedance measurements are shown as a function of inhibitor concentrations. The  $R_{ct}$  values increase and the  $C_{dl}$  values decrease with increasing concentration of the inhibitors and hence, the

inhibition efficiency (% IE) increases. The charge transfer resistance, which appeared to control the overall corrosion process, showed an increase with increasing inhibitor concentration. However, the capacity of the double layer decreased as inhibitor concentration increased. The double layer between charged metal surface and solution is considered as electrical capacitor and it is generally assumed that acid corrosion inhibitors adsorb on metal surface resulting in a structural change of double layer and reduced rate of electrochemical partial reaction. In the system under investigation, the decrease in electrical capacity of the working electrodes surface in the presence of the different inhibitors could be correlated with the decrease in the corrosive area on the electrodes surface owing to the increase of the area covered with the adsorbed inhibitor molecules [31].

**Table 7:** AC Impedance parameters for mild steel for selected concentrations of the inhibitors in 1M H<sub>2</sub>SO<sub>4</sub>.

Name of the Inhibitor	Inhibitor Concentration (mM)	R <sub>t</sub> (ohm cm <sup>2</sup> )	C <sub>dl</sub> (μ F cm <sup>-2</sup> )	Inhibition Efficiency (%)
Blank		11.06	36.8	-
PPM	0.5	17.56	24.3	37.01
	5	45.15	19.5	75.50
	10	50.32	20.06	78.02
PHPM	0.5	28.79	28.5	61.58
	5	51.26	29.5	78.42
	10	57.97	23.8	80.92
PAPM	0.5	23.22	22.9	52.36
	5	28.02	14.9	60.05
	10	66.66	10.4	83.40
PCT	0.5	37.49	27.2	70.49
	5	56.14	25.7	80.29
	10	70.50	27.2	84.31

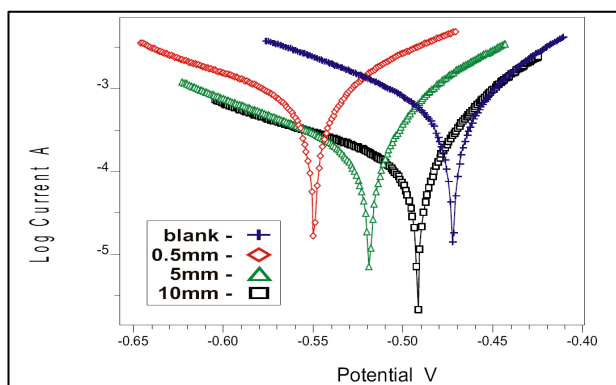


**Fig 4:** Polarization curve for mild steel recorded in 1M H<sub>2</sub>SO<sub>4</sub> for selected concentrations of inhibitor (PCT)

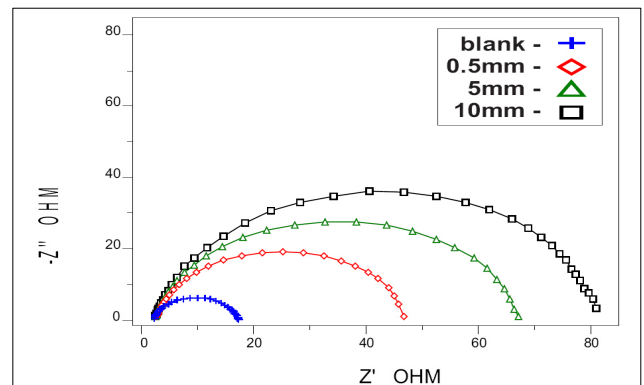


**Fig 5 :** Nyquist diagram for mild steel in 1M H<sub>2</sub>SO<sub>4</sub> for selected concentrations of inhibitor (PCT)

### 3.3.4 Scanning Electron Microscope-Energy Dispersive X-Ray Spectroscopy (SEM-EDX)

In order to evaluate the conditions of the mild steel surfaces in contact with acid solution, a superficial analysis was carried out. The SEM micrographs of mild steel specimen in 1M H<sub>2</sub>SO<sub>4</sub> solution in the absence and presence of inhibitors (PCT) after 3 hour exposure are given in (Figs. 6&7). As it is shown in (Fig. 6), the mild steel surface was strongly damaged in the absence of inhibitors due to metal dissolution in corrosive solution. However the appearance of steel surface was significantly different after the addition of inhibitors (PCT and PPCT) to the corrosive solution. It can be seen from (Fig. 7) that, the dissolution rate of mild steel considerably reduced and the smooth surface appeared by formation of a good protective film upon adsorption of inhibitor molecules on the metal surface, which was responsible for the inhibition of corrosion.

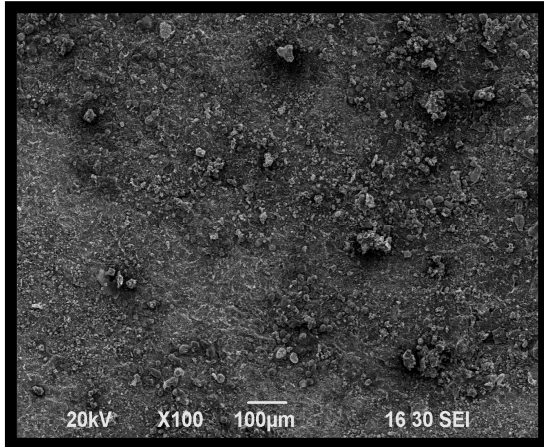


**Fig 6:** Blank

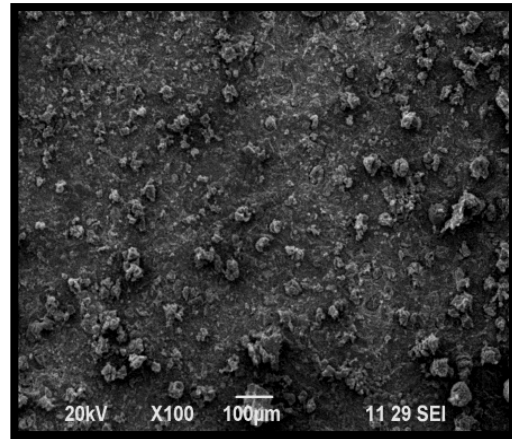


**Fig 7:** PCT

**Figs. 6&7** Scanning electron microscopy photographs in the absence and presence of inhibitor (PCT)

The EDX spectra was used to determine the elements present on the surface of mild steel in the uninhibited and inhibited 1M H<sub>2</sub>SO<sub>4</sub>. The EDX analysis of uninhibited mild steel plate indicate the presence of only Fe and oxygen confirming that passive film on the mild steel surface contained only Fe<sub>2</sub>O<sub>3</sub> (Fig. 8). EDX spectra of PCT (Fig. 9) show additional line and characteristic of N and S. In addition, the intensities of C and O signals are enhanced. The appearance of the N and S signal and this enhancement in the C and O signals confirms the presence of pyrazoline molecules on the metal surface. From the two EDS spectra, it is evident that the Fe peaks are considerably suppressed in the presence of inhibitors (PCT) which may be attributed due to the overlying inhibitor film [41]. A Comparable elemental distribution obtained from the spectra is presented in Table 8.

**Table 8:** Surface Composition (weight %) of mild steel after 3 hours of immersion in 1M without and with the optimum concentrations of the studied inhibitors [EDS Studies]

Mass (%)	Fe	C	N	O	S
Blank	66.20	-	-	33.80	-
PCT	46.93	5.16	7.03	40.14	0.74

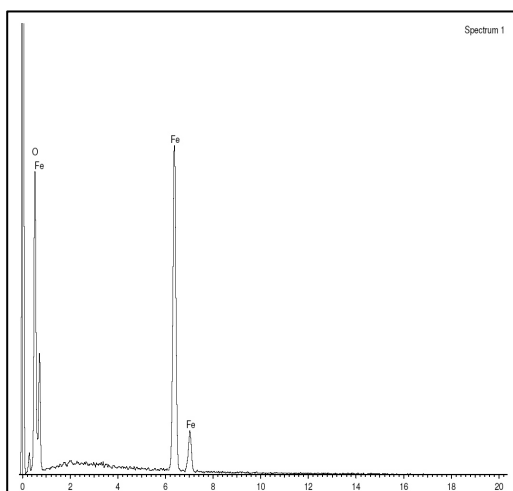


**Fig 8:** EDX spectra for mild steel in 1M H<sub>2</sub>SO<sub>4</sub> in absence of inhibitor

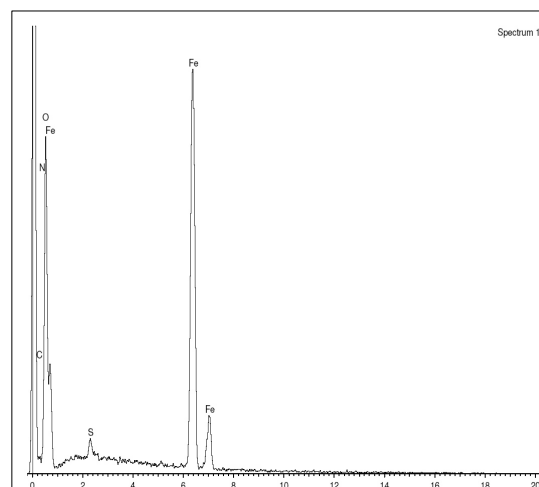


**Fig 9:** EDX spectra for mild steel in 1M H<sub>2</sub>SO<sub>4</sub> in presence of inhibitor (PCT)

### FT IR analysis of mild steel plate

Fig 10 shows the IR spectrum of the mild steel plates immersed in 10mM of PCT for 3 hours. All the peaks observed for the functional groups in the IR spectrum of the inhibitor OH, NH<sub>2</sub>, >C=S and >C=N around (3186.54cm<sup>-1</sup>, 3293.59 cm<sup>-1</sup>, 1246.07 cm<sup>-1</sup>, 1633.78 cm<sup>-1</sup>) are also found in the IR spectrum of the mild steel plates confirming the presence of the inhibitor on the mild steel surface. The IR spectrum of mild steel plates further substantiate the fact that the hydroxy pyrazolines are good corrosion inhibitors for mild steel in H<sub>2</sub>SO<sub>4</sub> medium.

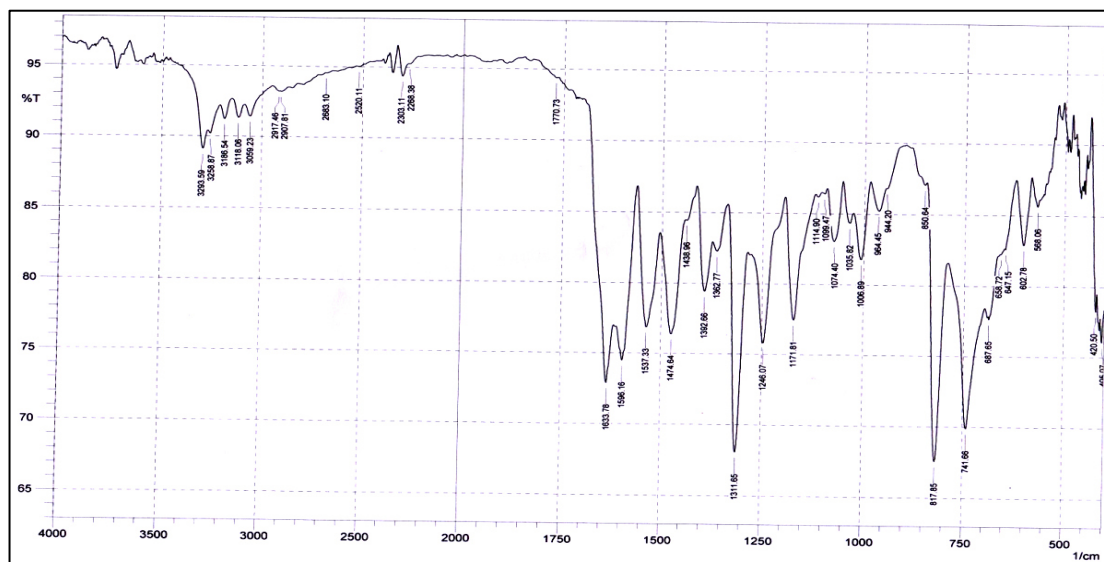


**Fig.10:** IR Spectrum of mild steel plate immersed in 1M H<sub>2</sub>SO<sub>4</sub> containing PCT

### 3.3.5 Quantum-chemical studies

In computational chemistry tools, the DFT offers the fundamentals for interpreting multiple chemical concept used in different branches of chemistry. Among quantum chemical methods for evaluation of corrosion inhibitors, density functional theory, DFT has shown significant promise and appears to be adequate for pointing out the changes in electronic structure responsible for inhibitory action. In order to explore the theoretical-experimental consistency, quantum chemical calculations were performed with complete geometry optimizations using standard Gaussian-03 software package. Geometry optimization was carried out by B3LYP functional at the 6-31G(d,p) basis set and at the density functional theory (DFT level). This basic set provide accurate geometry and electronic properties for a wide range of organic compounds. Recently, density functional theory (DFT) has been used to analyze the characteristics of the inhibitor/surface mechanism and to describe the structural nature of the inhibitor in the corrosion process. Furthermore, DFT is considered a very useful technique to probe the inhibitor/surface interaction as well as to analyze the experimental data. This technique has been found to be successful in providing insights into the chemical reactivity and selectivity in terms of global parameters such as electronegativity ( $\chi$ ), hardness ( $\eta$ ), softness (S) and local ones such as Fukui function, F(r) and local softness s(r).

The design of the hydroxy pyrazoline derivatives for use as corrosion inhibitor was based on several factors:

- (i) The molecule contains nitrogen, oxygen/sulphur atoms as active centers in addition to >C=O/>C=S, -NH, -OH and phenyl groups, which boasts not only biological functionality but also corrosion inhibition.
- (ii) Hydroxy pyrazolines can be easily synthesized and characterized. The optimized molecular structures of the synthesized hydroxy pyrazolines are presented in Table 10. Among the molecular properties that are well reproduced by DFT/B3LYP include the energy of the highest occupied molecular orbital (HOMO) energy of the lowest unoccupied molecular orbital (LUMO), electronegativity, global hardness and softness, electron affinity, ionization potential, etc.

### *Theoretical assessment*

To determine a relationship between inhibitors and their corresponding inhibition efficiency, quantum chemical calculations are used herein. Optimized geometric structures and Mulliken spin density plots of HOMO and LUMO for the inhibitors were studied which supported the corrosion inhibition efficiency obtained from experimental results [33]. Quantum chemical parameters obtained from the calculations which are responsible for the inhibition efficiency of inhibitors, such as the highest occupied molecular orbital ( $E_{\text{HOMO}}$ ), energy of lowest unoccupied molecular orbital ( $E_{\text{LUMO}}$ ), HOMO–LUMO energy gap ( $\Delta E$ ), dipole moment ( $\mu$ ) and total energy (TE), electronegativity ( $\chi$ ), electron affinity ( $A$ ), global hardness ( $\eta$ ), softness ( $\sigma$ ), ionization potential ( $I$ ), The global electrophilicity ( $\omega$ ), the fraction of electrons transferred from the inhibitor to iron surface ( $\Delta N$ ) and the total energy ( $TE$ ) are presented in Table 1.

The adsorption ability of the molecule over metal surface is related to their FMO (Frontier molecular orbital) i.e; highest molecular orbital (HOMO) and lowest unoccupied molecular orbital (LUMO). Excellent corrosion inhibitors are usually those compounds who not only offer electrons to unoccupied orbital of the metal, but also accept free electrons from the metal. It is important to focus on the parameters that directly influence the electronic interaction of the inhibitor molecules with the metal surface. These are mainly:  $E_{\text{HOMO}}$ ,  $E_{\text{LUMO}}$ ,  $\Delta E$  and  $\mu$ . Higher HOMO energy ( $E_{\text{HOMO}}$ ) of the molecule means a higher electron donating ability to appropriate acceptor molecules with low energy empty molecular orbital and thus explains the adsorption on metallic surfaces by way of delocalized pair of  $\pi$ -electrons,  $E_{\text{LUMO}}$ , the energy of the lowest unoccupied molecular orbital signifies electron receiving tendency of a molecule. The  $E_{\text{HOMO}}$  for the studied compounds follow the order; PCT > PAPM > PHPM > PPM which implies that the molecule which has the highest tendency to donate electrons is PCT. Energy gap ( $\Delta E$ ), is an important parameter as a function of reactivity of the inhibitor molecule towards the adsorption on the metallic surface. As  $\Delta E$  decreases the reactivity of the molecule increases which leads to increase in the % IE of the molecule. As for the values of  $\Delta E$  ( $E_{\text{LUMO}}-E_{\text{HOMO}}$ ) concern, lower values of the energy difference will cause higher inhibition efficiency because the energy required to remove an electron from the last occupied orbital will be low. A molecule with a low energy gap is more polarizable and is generally associated with the high chemical activity and low kinetic stability and is termed soft molecule. In our study, the trend for the ( $\Delta E$ ) values follow the order PCT > PAPM > PHPM > PPM, which suggests that PCT has the highest reactivity in comparison to other compounds and would therefore interact strongly with the metal surface [34].

There is lack of agreement in the literature on the correlation between the dipole moment and inhibition efficiency. It is shown from the calculations that there was no obvious correlation between the values of the dipole moment with the trend of inhibition efficiency obtained experimentally [35].

Electron density distributions was carried out by Natural bond orbital (NBO) analysis. In calculating the chemical reactivity parameters this electron density plays a very important role. The ionization potential and electron affinity of inhibitor molecules can be calculated by the application of Koopman's theorem [36]. This theorem shows a clear relationship between the HOMO and ionization potential; LUMO and electron affinity of the concerned molecule respectively. There is no formal authentication of this theorem within DFT, however, its validity has accepted since long back. The obtained ionization potential and electron affinity values are hereby used to get the electronegativity ( $\chi$ ) and global hardness ( $\eta$ ) of the molecule. High ionization energy indicates high stability and chemical inertness and small ionization energy indicates high reactivity of the atoms and molecules [37]. The low ionization energy 5.1065 (eV) of PCT indicates the high inhibition efficiency.

Absolute hardness and softness are important properties to measure the molecular stability and reactivity. It is apparent that the chemical hardness fundamentally signifies the resistance towards the deformation or polarization of the electron cloud of the atoms, ions or molecules under small perturbation of chemical reaction. A hard molecule has a large energy gap and a soft molecule has a small energy gap. In our present study PCT with low hardness value 1.8738 (eV) compared with other compound have a low energy gap. Normally, the inhibitor with the least value of global hardness (hence the highest value of global softness) is expected to have the highest inhibition efficiency. In the simple transfer of electrons, adsorption could occur at the part of the molecule where softness ( $\sigma$ ), which is a local property, has a higher value. PCT with the softness value of 0.5337 has the highest inhibition efficiency [38].

The absolute electronegativity is a chemical property that describes the ability of a molecule to attract electron towards itself in a covalent bond. According to Sanderson's electronegativity equalization principle [39], PHPM with a high electronegativity quickly reaches equalization and hence low reactivity is expected

which in turn indicates the low inhibition efficiency. From Table 9, it can be clearly seen that the PCT has the least electronegativity value (3.2327eV) and hence it is the best inhibitor

The electrophilicity index ( $\omega$ ), shows the ability of the inhibitor molecules to accept electrons. It is a measure of the stabilization in energy after a system accepts the additional amount of electron charge from the environment [40]. In our present study, PPM is the strongest nucleophile while PCT is the strongest electrophile.

**Table 9:** Calculated quantum chemical parameters of the optimized synthesized inhibitors.

Quantum chemical parameters	PPM	PHPM	PAPM	PCT
Total energy TE (amu)	-1164.49	-1239.71	-1219.84	-1311.76
Dipole moment $\mu$ (debye)	5.6240	5.6028	6.6860	8.1275
$E_{\text{HOMO}}$ (eV)	-5.8723	-5.8524	-5.3155	-5.1065
$E_{\text{LUMO}}$ (eV)	-1.3326	-1.4645	-1.3168	-1.3589
Energy gap, $\Delta E$ (eV)	4.5397	4.3879	3.9987	3.7476
Ionization potential (I)	5.8723	5.8524	5.3155	5.1065
Electron affinity (A)	1.3326	1.4645	1.3168	1.3589
Electronegativity ( $\chi$ )	3.6025	3.6585	3.3162	3.2327
Hardness ( $\rho$ )	2.2699	2.1940	1.9994	1.8738
Softness ( $\sigma$ )	0.4406	0.4558	0.5002	0.5337
Electrophilicity index ( $\omega$ )	6.96713	7.1539	11.1790	17.6263
$\Delta N$ (No of electrons transferred)	0.7484	0.7615	0.9213	1.005

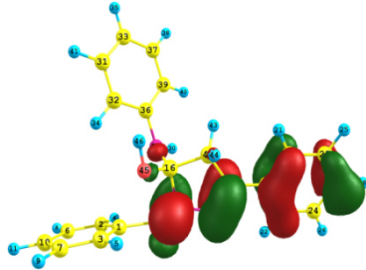
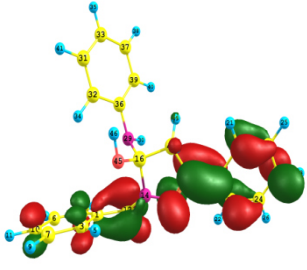
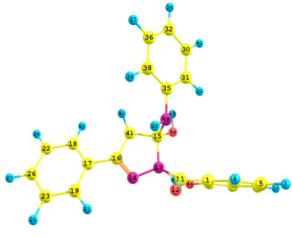
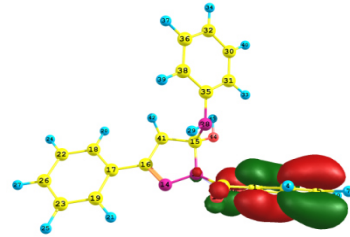
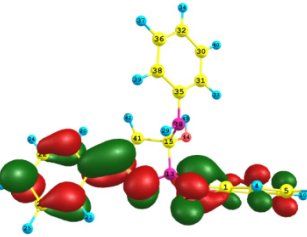
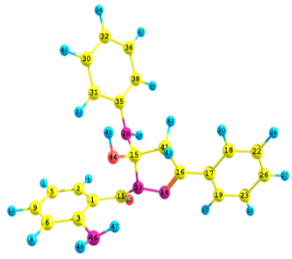
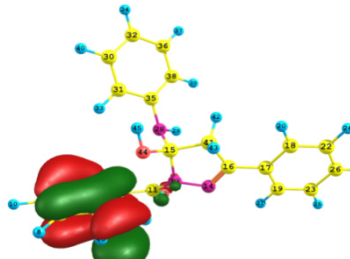
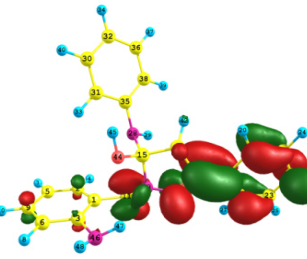
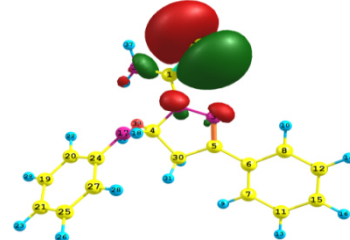
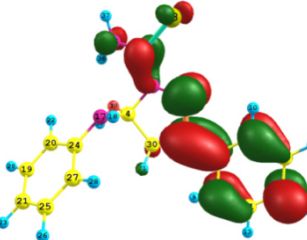
To calculate the fraction of electrons transferred, the theoretical values of  $\chi$  (Fe) = 7 eV and  $\eta$  (Fe) = 0 eV are used [41]. Generally, value of  $\Delta N$  indicates the electron donating capacity of the inhibitors, and the inhibition efficiency increases with the increase in electron donating ability to the metal surface. According to Lukovits's study [42], if  $\Delta N < 3.6$ , the inhibition efficiency increases with increasing electron donating ability at the metal surface. Based on these calculations, it is expected that the synthesized inhibitor is a donor of electrons, and the steel surface is the acceptor, and this favors chemical adsorption of the inhibitor on the electrode surface. Here the inhibitor binds to the steel surface and forms an adsorption layer against corrosion. The synthesized inhibitor PCT shows the highest inhibition efficiency because it has the highest HOMO energy and this reflects the greatest ability (the lowest  $\Delta E$ ) of offering electrons.

#### Local reactivity of the selected corrosion inhibitors

To establish the active site of an inhibitor molecule, three influencing and controlling factors: neutral atomic charge, distribution of frontier molecular orbital and Fukui indices are considered. Local reactivity is analyzed by means of the condensed Fukui function. Condensed Fukui functions allow us to distinguish each part of the molecule on the basis of its distinct chemical behavior due to the different substituent functional groups. The nucleophilic and electrophilic attack is controlled by the maximum values of  $f_k^+$  and  $f_k^-$ . The calculated Fukui indices for nucleophilic and electrophilic attack for the synthesized inhibitors are tabulated in Table 11a-11d Parr and Yang proposed that larger value of Fukui function indicates more reactivity [43]. Hence greater the value of condensed Fukui function, the more reactive is the particular atomic center of the molecule.

The  $f_k^+$  measures the changes of density when the molecules gain electrons, and it corresponds to reactivity with respect to nucleophilic attack. On the other hand,  $f_k^-$  corresponds to reactivity with respect to electrophilic attack or when the molecule lose electrons. From the results it is evident that the site for nucleophilic attack in PPM, PAPM, PHPM and PCT are in N14, N46, N46 and S38 respectively. On the other hand, the sites for electrophilic attack are in O13, O12, O12 and S38 respectively. In case of PCT, the electrophilic and nucleophilic attack are found in  $>C=S$ .

**Table 10:** The 3D-structure of the studied inhibitors

inhibitor	Optimized structure	HOMO	LUMO
PPM			
PHPM			
PAPM			
PCT			

**Table 11a:** Calculated Mulliken atomic charges, Fukui functions and softness indices for the atoms of PPM using DFT at the B3LYP/6-31G(d,p) basis set

Atoms	$q_N$	$q_{N+1}$	$q_{N-1}$	$f_k^+$	$f_k^-$	$S_k^+$	$S_k^-$
O13	-0.4603	-0.4005	-0.5276	0.0598	0.0673	0.0263	0.0296
N14	-0.3888	-0.3281	-0.3836	0.0607	-0.0052	0.0268	-0.0023
N15	-0.2824	-0.2390	-0.3334	0.0435	0.0014	0.0192	0.0225
N29	-0.297	-0.2575	-0.2906	0.0395	-0.0064	0.0174	-0.0028

### 3.3.6 Mechanism of corrosion inhibition

The adsorption of pyrazoline derivatives can be attributed to the presence of polar unit having atoms of nitrogen, oxygen, sulphur and aromatic/heterocyclic rings. Therefore the possible reaction centers are unshared electron pairs of heteroatoms and  $\pi$ -electrons of aromatic ring [44]. Corrosion inhibition of mild steel in 1M  $H_2SO_4$  by pyrazolines can be explained on the basis of molecular adsorption onto the metal/solution interface. In aqueous acidic solutions, pyrazoline derivatives exist either as neutral molecules or as protonated molecules and may adsorb on the metal/acid solution interface by one and/or more of the following ways:

- i. Electrostatic interaction of protonated molecules with already adsorbed sulphate ions.
- ii. Donor-acceptor interactions between the  $\pi$ -electrons of aromatic rings and vacant d-orbital of surface iron atoms.
- iii. Interaction between unshared electron pairs of hetero-atoms and vacant d-orbital of iron surface atoms.

**Table 11b:** Calculated Mulliken atomic charges, fukui functions and softness indices for the atoms of PPHM using DFT at the B3LYP/6-31G(d,p) basis set

Atoms	$q_N$	$q_{N+1}$	$q_{N-1}$	$f_k^+$	$f_k^-$	$S_k^+$	$S_k^-$
O12	-0.4621	-0.4217	-0.5314	0.0404	0.0693	0.0184	0.0316
N13	-0.4821	-0.4709	-0.4758	0.0112	-0.0063	0.0051	0.0029
N14	-0.2766	-0.2516	-0.3247	0.0249	0.0482	0.0114	0.0220
N28	-0.2959	-0.2674	-0.2875	0.0285	-0.0084	0.0130	-0.0038
N44	-0.2260	-0.2095	-0.2473	0.0165	0.0213	0.0515	0.0097
N46	-0.2200	-0.1345	-0.2517	0.0854	0.0318	0.0389	0.0145

**Table 11c:** Calculated Mulliken atomic charges, fukui functions and softness indices for the atoms of PAPM using DFT at the B3LYP/6-31G(d,p) basis set

Atoms	$q_N$	$q_{N+1}$	$q_{N-1}$	$f_k^+$	$f_k^-$	$S_k^+$	$S_k^-$
O12	-0.4529	-0.4116	-0.5135	0.0413	0.0606	0.0207	0.0303
N13	-0.4171	-0.4099	-0.4132	0.0072	-0.0038	0.0036	-0.0019
N14	-0.2788	-0.2612	-0.3387	0.0176	0.0599	0.0088	0.0300
N28	-0.2940	-0.2867	-0.2904	0.0073	-0.0036	0.0036	-0.0018
O44	-0.2354	-0.2292	-0.2582	0.0062	0.0228	0.0031	0.0114
N46	-0.1326	0.0372	-0.1641	0.1699	0.0315	0.0850	0.0157

**Table 11d:** Calculate Mulliken atomic charges, fukui functions and softness indices for the atoms of PCT using DFT at the B3LYP/6-31G(d,p) basis set

Atoms	$q_N$	$q_{N+1}$	$q_{N-1}$	$f_k^+$	$f_k^-$	$S_k^+$	$S_k^-$
N2	-0.3337	-0.2887	-0.3286	0.045	-0.0051	0.024	-0.0027
N3	-0.2779	-0.2813	-0.3505	-0.0033	0.0726	-0.0018	0.0387
N17	-0.2761	-0.2675	-0.2878	0.0086	0.0117	0.0046	0.0062
O33	-0.2273	-0.1987	-0.2571	0.0286	0.0298	0.0152	0.0159
N35	0.0109	0.1027	-0.059	0.0918	0.0688	0.0490	0.0367
S38	-0.2858	0.0992	-0.4144	0.3850	0.1286	0.2055	0.0686

In general, two modes of adsorption are considered on the metal surface in acid media. In the first mode, neutral molecules may be adsorbed on the surface of mild steel through the chemisorptions mechanism, involving the displacement of water molecules from the mild steel surface and the sharing electrons between the hetero-atoms and iron. The inhibitor molecules can also adsorb on the mild steel surface on the basis of donor-acceptor interactions between  $\pi$ -electrons of the aromatic ring and vacant d-orbitals of surface iron atoms. In the second mode, since it is well known that the steel surface bears positive charge in acid solution [45], it is difficult for the protonated molecules to approach the positively charged steel surface due to the electrostatic repulsion. But sulphate ions have a smaller degree of hydration and these ions could bring excess negative charges in the vicinity of the interface and favor more adsorption of the positively charged inhibitor molecules. The protonated pyrazolinium ion adsorb through electrostatic interactions between the positively charged molecules and the negatively charged metal surface. Thus, we can conclude that inhibition of mild steel corrosion in 1M H<sub>2</sub>SO<sub>4</sub> is mainly due to electrostatic interaction. The decrease in inhibition efficiency with rise in temperature supports electrostatic interaction.

### Conclusions

- All investigated pyrazolines are effective inhibitors for the corrosion of mild steel in 1M H<sub>2</sub>SO<sub>4</sub>.
- The high inhibitive effect of pyrazolines were attributed to the adherent adsorption of the inhibitor molecules on the metal surface and a protective film formation.
- Adsorption mechanism of the pyrazolines on mild steel in 1M H<sub>2</sub>SO<sub>4</sub> solution at 30°C was a combination of both physisorption and chemisorption.
- Adsorption of the investigated pyrazolines fitted Langmuir isotherm model.
- Polarization curves indicated that all the synthesized pyrazolines behaves mainly as mixed inhibitor but predominantly act as cathodic type.
- Impedance method indicate that pyrazoline molecules adsorbed on the mild steel surface with increasing transfer resistance and decreasing the double layer capacitance
- SEM micrographs of mild steel specimen showed that the inhibitor molecules form a good protective film on the metal surface.
- Theoretical studies correlate with the experimental studies.

**Acknowledgment**-The authors declare no competing financial interest

## References

1. Amin M.A., Khaled K.F., Mohren Q., Arida H.A., *Corros. Sci.*, 52 (2010) 1684.
2. Veawab A., P. Tontiwachwuthikul, A. Chakma, *Ind. Eng. Chem. Res.*, 38, (1999), 3917.
3. Touhami F., A. Aouniti, A. Abed, B. Hammouti, S. Kertit, A. Ramdani, K. Elkacemi, *Corros. Sci.*, 42, (2000), 929.
4. Lal B., Y. Zhou, P. Yang, *Ind. Eng. Chem. Res.*, 51, (2012), 7777.
5. Zerfaoui M., H. Oudda, B. Hammouti, S. Kertit, M. Benkaddour, *Prog. Org. Coat.*, 51, (2004), 134.
6. Feng Y., S. Chen, W. Guo, Y. Zhang, G. Liu, *J. Electroanal. Chem.*, 602, (2007), 115.
7. Zhang Z., S. Chn, Y. Li, S. Li, L. Wang, *Corros. Sci.*, 51, (2009), 29.
8. Colorado-Garrido D., D. M. Ortega-Toledo, J. A. Hernandez, J. G. Gonzalez-Rodriguez, J. Uruchurtu, *J. Solid state Electrochem.*, 13, (2009), 175.
9. Lukovits I., E. Kalman, F. Zucchi, *Corrosion.*, 57 (2001), 3.
10. Prabodh Chander Sharma, Sunil V. Sharma, Sandeep Jain, Dalbir Singh and Bhojraj Suresh, *Acta Pol. Pharm.*, 66(1), (2009), 101-104.
11. Seranthimata Samshuddin, Badiadka Narayana, Balladka Kunhanna Sarojini, Rajagopalan Srinivasan, Vinayachandra, K.R. Chandrashekar, *Der Pharma Chemica.*, 4 (2), (2012), 587-592.
12. Ali S.A., A.M. El-Shareef, R.F. Al-Ghandi, M.T. Saeed, *Corros. Sci.*, 47 (2005), 2659-2678.
13. Abboud Y., A. Abourriche, T. Saffaj et al, *Desalination*, 237(1-3), (2009), 175-189.
14. Every R.L., O.L. Riggs, *Mat.Prot.*, 3, (1964), 46.
15. Ahamad I., R. Prasad, M.A. Quraishi, *Corros. Sci.*, 52, (2010), 3033.
16. Popova A., *Corros. Sci.*, 49, (2007), 2144.
17. El-Etre A.Y., *J. Colloid interf. Sci.*, (2007), 578.
18. Qu Q., S. Jiang, W. Bai, L. Li, *Electrochim. Acta*, 52 (2007), 6811.
19. Herrag L., B. Hammouti, S. Elkadiri, A. Aoumt, C. Jama, H. Vezin, F. Bentiss, *Corros. Sci.*, 52 (2010), 3042.
20. Singh A.K., S.K. Shukla, M.A. Quraishi, E.E. Ebenso, *J. Taiwan Inst. Chem. Eng.*, 43 (2012), 463-472.
21. Khadom A.A., A.S. Yaro, A.S. Altaie, A.A.H. Khadum, *Port. Electrochim. Acta*, 27(6) (2009), 699-712.
22. Wang L., *Corros.Sci.*, 43, (2001), 1637-1644.
23. Zhang Q.B., Y.X. Hua, *Electrochimica. Acta*, 54, (2009), 1881-1887.
24. Bayol K., Kayakirilmaz M., Erbil, *Mater. Chem. Phys.*, 104, (2007), 74-82.
25. R. Touir, R. A. Belakhmima, M. Ebn Touhami, L. Lakhrissi, M. El Fayed, B. Lakhrissi, E. M. Essassi, *J. Mater. Environ. Sci.* 4(6) (2013) 921-930
26. Zhao T.P., G.N.Mu, *Corros. Sci.*, 41, (1999), 1937-1944.
27. Jeyaperumal D., *Mater. Chem. Phys.*, 119, (2010), 478-481.
28. Ferreira E. S., C. Glancomlli, F. C. Glacomelli, A. Spinelli, *Mater. Chem. Phy.*, 83, (2004),129-134.
29. Jones DA. Principles and Prevention of Corrosion, second ed. Prentice Hall, Upper Saddle River, NJ. P. 518 (1996).
30. F.ansfeld F, *Electrochim. Acta*. 35 (1990)1533.
31. Mahmoud S.S., M. M. Ahmed, R.A. El-Kasaby, *Adv. Mater. Corros.* 1, (2013), 36-45.
32. Fouda A.S., S.Rashwan and Y.K.Elghazy, *Int. J.Adv. Res*, 1(10), (2013), 568-589.
33. Deng S., X.Li, h.Fu, *Corros.Sci.*, 53, (2011), 822-828.
34. Udayakala P, T.V.Rajendran T V, S. Gunasekaran, *J. Comput. Methods Mol. Des.*, 2(1), (2012), 1-15.
35. Udhayakalaa P., T. V. Rajendiran, S. Gunasekaran, *Der Pharmacia Lettre*, 4 (4), (2012), 1285-1298.
36. Karzazi Y., El Alaoui Belghiti M., Dafali A., Hammouti B., *J. Chem. Pharm. Res.*, 6(4) (2014) 689-696
37. Chakraborty T., D.C.Ghosh, *Mol. Phys*, 108( 16), (2010), 2081-2092.
38. Zarrouk A., H. Zarrok, R.Salghi, B.Hammouti, S.S. Al-Deyab, R.Touzani, M.Bouachrine, I. Warad, T.B.Hadda, *Int. J. Electrochem. Sci.*, 7 (2012) 6353 – 6364
39. Geerlings P., F. De Proft., *Int. J. Mol. Sci.* (2002) 3, 276-309.
40. Liu S., *J Chem Sci*, 117, (2005), 477-481.
41. Zarrok H., A. Zarrouk, R. Salghi, H. Oudda, B. Hammouti, M. Assouag, M. Taleb, M. Ebn Touhami, M. Bouachrine and S. Boukhris, *J. Chem. Pharm. Res.*, 4(12), (2012), 5056-5066.
42. Khadraoui A., Khelifa A., Boutoumi H., Mettai B., Karzazi Y., Hammouti B., *Port. Electrochim. Acta*, 32 (2014) 271-280
43. Parr R.G., W. Yang, *Density Functional Theory of Atoms and Molecules*; Oxford University Press, (1989).
44. Ishtiaque Ahamad, Rajendra Prasad, M.A. Quraishi, *Corros. Sci.*, 52 (2010), 3033.
45. Hammett L.P., *Physical Organic Chemistry*, McGraw-Hill Book Co., New York

(2015) ; <http://www.jmaterenvirosci.com>